Published in final edited form as:
J Cell Physiol. 2009 May ; 219(2): 430–437. doi:10.1002/jcp.21686.

Lack of lymphatic vessel phenotype in LYVE-1/CD44 double knock out mice

Mai X. Luong[†,1,§], **Joshua Tam**[†,1,2], **Qingcong Lin**[†,3], **Jeroen Hagendoorn**[1,#], **Kathryn J. Moore**[4], **Timothy P. Padera**[1], **Brian Seed**[5], **Dai Fukumura**[1], **Raju Kucherlapati**[*,6], and **Rakesh K. Jain**[*,1]

1*Department of Radiation Oncology, Massachusetts General Hospital, Charlestown, MA 02129*

2*Harvard-MIT Division of Health Sciences and Technology, Massachusetts Institute of Technology, Cambridge, MA 02139*

3*Molecular Genetics, Biological Technologies, Wyeth Research, Cambridge, MA 02140*

4*Department of Lipid Metabolism, Massachusetts General Hospital, Boston, MA 02114*

5*Department of Genetics, Massachusetts General Hospital and Harvard Medical School*

6*Harvard Medical School-Partners Healthcare Center for Genetics and Genomics, Harvard Medical School, Boston, MA 02115*

Abstract

Lymphatic vessels play a key role in maintaining tissue-fluid homeostasis, immune surveillance and metastasis. The hyaluronan receptor, LYVE-1, is widely used as a molecular marker for adult and embryonic lymphatic endothelium, but its physiological functions have not yet been established *in vivo*. In agreement with a recent report, LYVE-1$^{-/-}$ mice, which are healthy and fertile, do not display any defects related to congenital abnormalities of the lymphatic system. One hypothesis for the absence of a phenotype in LYVE-1 null mice is that other hyaluronan receptors, such as CD44, may compensate for LYVE-1. To test this hypothesis, we created LYVE-1/CD44 double knockout mice with appropriate littermate controls. Lymphatic vessel structure and function, as determined by histological methods and intravital microscopy, show that LYVE-1$^{-/-}$, CD44$^{-/-}$ and LYVE-1$^{-/-}$/CD44$^{-/-}$ mice are indistinguishable from wild-type mice under normal conditions. Furthermore, resolution of carrageenan-induced paw edema is comparable in all genotypes. However, LYVE-1$^{-/-}$/CD44$^{-/-}$ mice exhibit increased edema formation in a carrageenan-induced paw inflammation model compared to wild-type mice, but not to LYVE$^{-/-}$ or CD44$^{-/-}$ mice. These data suggest that LYVE-1 and CD44 are not required for the formation or function of lymphatics, but do not rule out a role for LYVE-1 in inflammation.

Keywords

Lymphatic vessels; LYVE-1; CD44

*Corresponding authors: Rakesh K. Jain, PhD, A.W. Cook Professor of Tumor Biology, Massachusetts General Hospital, Department of Radiation Oncology-Cox 7, 100 Blossom St., Boston, MA 02114, Tel: 617-726-4083, Fax: 617-724-1819, jain@steele.mgh.harvard.edu, AND, Raju Kucherlapati, PhD, Paul C. Cabot Professor of Genetics, Harvard Medical School, Center for Genetics and Genomics #250, 77 Louis Pasteur Ave, Boston, MA 02115, Tel: 617-525-4445, Fax: 617-5252-4440, rkucherlapati@PARTNERS.ORG.

†Mai X. Luong, Joshua Tam and Qingcong Lin contributed equally to this study.

§current address: Department of Cell Biology, University of Massachusetts Medical School, Worcester, MA 01655

#current address: Department of Surgery, University Medical Center, Utrecht, The Netherlands

INTRODUCTION

The lymphatic system comprises a network of vessels that maintain tissue homeostasis by collecting interstitial fluid and proteins from the surrounding tissues and transporting them to the blood (Schmid-Schonbein, 1990). Abnormalities in lymphatic vasculature that cause inadequate drainage can lead to lymphedema, a condition characterized by swelling of the tissues that results from protein and fluid accumulation in the interstitium (reviewed in reference (Saharinen et al., 2004)). Vessels of the lymphatic system are also critical for immune surveillance as they transport dendritic cells to lymph nodes, a primary site for antigen presentation. In addition to leukocyte trafficking, lymphatic vessels also serve as a conduit for the metastatic spread of tumor cells to distant sites (reviewed in reference (Alitalo and Carmeliet, 2002)). Recent studies suggest that growth of lymphatic vessels—lymphangiogenesis—can contribute to tumor metastasis (Achen et al., 2005; Alitalo and Carmeliet, 2002). The molecular mechanisms that regulate the development of lymphatic vessels and their function are being elucidated as molecular markers that allow the identification and isolation of lymphatic endothelium have been characterized, including Prox-1, podoplanin, vascular endothelial growth factor receptor-3 (VEGFR-3), and lymphatic vessel endothelial hyaluronan receptor-1 (LYVE-1). Lymphatic endothelial cells have distinct transcriptional profiles from blood vascular endothelial cells, including in cell adhesion molecules, cytokines and cytokine receptors (Nelson et al., 2007).

Expression of Prox-1 and podoplanin is essential for the normal development of the lymphatic system (Schacht et al., 2003; Wigle and Oliver, 1999), while the VEGF-C/VEGFR-3 signaling pathway is required for embryonic lymphatic sprouting (Karkkainen et al., 2004). In contrast, the *in vivo* functions of LYVE-1 are not known (Gale et al., 2007; Jackson, 2004). Although the expression pattern of LYVE-1 in embryonic and adult lymphatic tissue suggests a role for LYVE-1 in the formation and function of the lymphatic system, a recent report shows normal lymphatic development and function in LYVE-1 deficient mice (Gale et al., 2007). The lack of a lymphatic phenotype suggests either that LYVE-1 is dispensable for development of the lymphatic system, or that LYVE-1 function is compensated by other receptor(s) (Gale et al., 2007).

LYVE-1 is a transmembrane receptor that belongs to a family of proteins that binds the large extracellular matrix mucopolysacharide hyaluronan (HA) through a conserved Link domain. Together with Prox-1 and podoplanin, LYVE-1 is expressed during embryogenesis on endothelial cells that bud off from the cardinal vein to form primitive lymph sacs (Wigle et al., 2002), however, LYVE-1 is also expressed on blood vessel endothelial cells in early embryogenesis and persists on endothelial cells of the lung and endocardium throughout embryogenesis (Gordon et al., 2008). In adults, LYVE-1 is expressed on initial lymphatic vessels and hepatic sinusoidal endothelium (Makinen et al., 2005; Mouta Carreira et al., 2001; Prevo et al., 2001). LYVE-1 can bind immobilized HA *in vitro* (Banerji et al., 1999) and can mediate internalization of labeled HA by transfected fibroblasts (Banerji et al., 1999; Prevo et al., 2001). However, little HA is bound to LYVE-1 in the majority of lymphatic vessels, suggesting that the HA-binding status of LYVE-1 in normal tissues is in the “off” state (Banerji et al., 1999).

HA plays a vital role in cell migration, both during embryonic morphogenesis and postnatal processes such as wound healing and cancer metastasis (Knudson and Knudson, 1993). HA undergoes high turnover, and partially degraded HA products act as proinflammatory factors that induce angiogenesis (West et al., 1985), stimulate chemokine production (McKee et al., 1996) and recruit dendritic cells (Termeer et al., 2000). Under normal conditions, HA and its breakdown products are maintained at very low levels in blood but are relatively high in lymph

(Knudson and Knudson, 1993). HA is cleared by the liver and to some extent by lymph nodes. Local HA levels rise in response to infection, injury or neoplasia.

A role for LYVE-1 during inflammation and metastasis is suggested by its high (43%) similarity to CD44, the other cell-surface HA-receptor in the Link family. CD44 is expressed on leukocytes and broadly in epithelial cells including cancer cells, and is mostly absent from lymphatic endothelium. During inflammation, interactions of CD44 with HA facilitate leukocyte adhesion to and subsequent migration across inflamed vascular endothelium, which has increased HA biosynthesis. Consistent with this observation, HA binding activity by CD44 is low under normal conditions, but can be induced by inflammatory cytokines. Similarly, it is possible that LYVE-1 functions to regulate leukocyte migration in the lymphatic system through its interaction with HA at the luminal and abluminal surfaces, which would serve as a pathway for intravasation of $CD44^+$ leukocytes. Interestingly, inflammatory cytokines modulate the expression levels of LYVE-1, rather than its HA-binding activity (Jackson, 2004). Depending on the timing of LYVE-1 upregulation or activation of HA-binding activity, it is possible that LYVE-1 may instead participate in resolving inflammation, by binding or internalizing HA and sequestering it away from leukocytes (Jackson, 2004). In addition to a role in immune responses, it is possible that LYVE-1, like CD44, also plays a key role in tumor metastasis by facilitating lymphatic intravasation of $CD44^+$ cancer cells en route to lymph nodes.

To investigate the *in vivo* functions of LYVE-1 in the lymphatic and immune systems, we inactivated the *LYVE-1* gene in the mouse by homologous recombination. In agreement with a recent report (Gale et al., 2007), *LYVE-1*-deficient ($LYVE^{-/-}$) mice are healthy and have a functional lymphatic system. To test whether LYVE-1 deficiency is compensated by its closest homologue (Gale et al., 2007), CD44, we generated *LYVE-1/CD44* double knockout mice. Wild-type, $CD44^{-/-}$, $LYVE^{-/-}$ and $CD44^{-/-}/LYVE^{-/-}$ mice are indistinguishable in appearance and showed no lymphatic defects. Lymph velocity in these mice is normal and the resolution of carrageenan-induced paw edema is comparable in all mice. However, $CD44^{-/-}/LYVE^{-/-}$ mice exhibit enhanced carrageenan-induced edema compared to wild-type mice, but not compared to $CD44^{-/-}$ or $LYVE^{-/-}$ mice. Together the findings presented here suggest that LYVE-1 and CD44 are not required for the formation or function of lymphatics, but do not rule out a role for LYVE-1 in inflammation.

MATERIALS AND METHODS

Construction of the *LYVE-1* targeting vector

The gene targeting vector was constructed from a bacterial artificial chromosome (BAC) clone that contains the *LYVE-1* locus on a C57BL/6J mouse genomic insert (RP23-34M19, GenBank accession number AZ238936). To replace exons 2 and 3 of the *LYVE-1* gene in the BAC clone with a neomycin resistance (neo) gene, the BAC clone was modified with a neo cassette by homologous recombination in *E. coli* EL250 cells as described previously (Lee et al., 2001). The neo gene was driven both by eukaryotic (PGK) and prokaryotic (EM7) promoters and thus allowed for positive selection of targeted clones in mammalian and bacterial cells. Correctly targeted BAC clones, identified by multiple restriction enzyme mapping, were further modified to insert a thymidine kinase cassette 3' of exon 6, which allowed for negative selection (Fig. 1A). The final targeting construct contained a 2.3-kb (from exon 1 to intron 1) and 7.4-kb (from intron 3 to exon 6) fragment of the *LYVE-1* gene flanking the neo cassette.

Transfection of Embryonic Stem Cells and Generation of $LYVE\text{-}1^{-/-}$ Mice

Mice with a modified *LYVE-1* locus were generated by homologous recombination in J1 embryonic stem cells transfected with NotI-digested targeting vector (50 mg) by

electroporation. Clones were screened by long-range PCR analysis using primer PF (5'-ccagaaagccatccacaaagtacag-3'), corresponding to sequences 5' of exon 1, and primer Neo-PR (5'- tacccggtagaatttcgacgacct-3'). Positive clones were confirmed by Southern blot analysis of SspI-digested genomic DNA using an 856-bp PCR product amplified with primers UF (5'-aaaaccccgcttggagatac-3') and UR (5'-gctgactcagaaagcacacg -3') as a probe. The wild-type allele was detected as a 4.2-kb fragment, whereas the mutant allele produced a 6.2-kb fragment. To generate chimeric mice, two ES clones heterozygous for the *LYVE-1* gene were used for microinjection into C57BL/6 blastocysts. Germline transmission was observed upon breeding of chimeric mice with C57BL/6 mice.

Generation of *LYVE-1*/*CD44* double KO mice

Homozygous *CD44* deficient 129 mice were obtained from the Jackson Laboratory (Bar Harbor, Maine) (Protin et al., 1999). $CD44^{-/-}$ mice were crossed with $LYVE\text{-}1^{-/-}$ mice. $LYVE\text{-}1^{+/-}/CD44^{+/-}$ mice were used for breeding. All litters were genotyped for *LYVE-1* and *CD44* genes. Wild-type ($LYVE\text{-}1^{+/+}/CD44^{+/+}$), $LYVE\text{-}1^{-/-}$ ($LYVE\text{-}1^{-/-}/CD44^{+/+}$), $CD44^{-/-}$ ($LYVE\text{-}1^{+/+}/CD44^{-/-}$), $LYVE\text{-}1^{-/-}/CD44^{-/-}$ mice were identified and used for the experiments.

Genotyping

Progeny from *LYVE-1* heterozygous pair matings were genotyped by PCR analysis of tail/toe DNA using primer pair CF1/CR2 (CF1, 5'-aaagtcgacttgactgatttgcacggatt-3'; CR2, 5'-aaagcggccgcatgtaaggaagcctccgaga-3') to detect the wild-type allele as a 1056-bp product, and primer pair CF1/PGK-R2 (PGK-R2, 5'- taaagcgcatgctccagact -3') to detect the *LYVE-1* mutant allele as a 700-bp product. The three primers can be put together in one PCR reaction. The PCR profile used was 1 cycle of 95°C for 5 min, followed by 30 cycles of 94°C for 30 s, 57° C for 30 s, and 72°C for 30 s, followed by 72°C for 10 min and then, 4°C. Progeny from $CD44^{+/-}$ matings were genotyped by PCR analysis of toe/tail DNA using primer pair CD44 F/CD44 R (CD44 F, 5'-ggcgactagatccctccgtt-3'; CD44 R, 5'-acccagaggcataccagctg-3') to detect the wild-type allele as a 175-bp product, and primer pair lacZ ROSA 26F/lacZ ROSA 26R (lacZ ROSA 26F, 5'-ttcactggccgtcgttttacaacgtcgtga-3'; lacZ ROSA 26R, 5'-atgtgagcgagtaacaacccgtcggattct-3') to detect the lacZ allele as a 364-bp product. The PCR profile used was 1 cycle of 95°C for 5 min, followed by 12 cycles of 94°C for 20 s, 64°C for 30 s, and 72°C for 35 s, followed by 25 cycles of 94°C for 20 s, 58°C for 30 s, 72°C for 35 s, followed by 72°C for 2 min and then, 4°C.

Western blot analysis

Protein from lung tissue were extracted by homogenization with a Dounce Homogenizer (Wheaton Science Products, Millville, NJ) in ice-cold RIPA buffer (Boston BioProducts, Inc., Worcester, MA) containing Complete Mini Protease Inhibitor Cocktail (Roche, Basel, Switzerland) and the concentration was determined using the Dc Protein Assay Reagents (BioRad Laboratories, Hercules, CA) according to the manufacturer's instructions. Protein (20 μg) were subjected to SDS-polyacrylamide gel electrophoresis and transferred to Immobilon Transfer Membrane (Millipore Corporation, Billerica, MA). Membranes were probed with rabbit anti-LYVE-1 antibody (1:1,000 dilution, Upstate Biotechnology, Lake Placid, NY) raised against amino acids 267–284. Detection of LYVE-1 protein was carried out with donkey anti-rabbit antibody conjugated to horseradish peroxidase (1:5,000 dilution, Santa Cruz Biotechnology, Santa Cruz, CA) and chemiluminescence detection (ECL Western Blotting Detection Reagents, Amersham Biosciences, Piscataway, NJ). Membranes were stripped for 15 minutes at 65°C with Restore Western Blot Stripping Buffer (Pierce Biotechnology, Rockford, IL) and re-blotted with goat anti-β actin antibody (1:1,000 dilution, Santa Cruz Biotechnology).

Quantitative Measurements of Lymphatic Flow Rate Using Residence Time Distribution Analysis

Transport in lymphatic capillaries was analyzed using residence time distribution theory as described previously (Swartz et al., 1996). Briefly, mice were anesthetized with ketamine/xylazine, and the tip of the tail was intradermally injected with FITC-dextran (2.5%) (MW=2 million, Sigma-Aldrich, St. Louis, MO) in PBS with a constant pressure of 40 cm H_2O via a 30-gauge needle. Beginning at the distal end of the tail, an epifluorescence microscope was used to image 8 adjacent regions every 10 minutes until saturation was reached at the proximal region. Temporally consecutive images, with a dimension of 3.5 × 2.5 mm, were subsequently analyzed using NIH Image Analysis software. Each image was subdivided into 10 equal sections equaling 0.35 mm of tail in the axial direction and the average fluorescence intensity for each section was determined. The temporal change in intensity in each section was used to calculate the mean residence time, which then is used calculate the lymphatic network filling velocity. Images of fluorescent vessels were also used to determine lymphatic vessel diameter and density as described previously (Jeltsch et al., 1997).

Ear microlymphangiography

To visualize lymphatic vessels in the ear, 2 μl FITC-dextran (2.5%) (MW=2 million, Sigma) in normal saline was slowly injected intradermally into the tip of the ear of anesthetized mice and imaged with epifluorescence microscopy.

Carrageenan-induced paw edema

Mice were anesthetized and paw edema was induced by subplantar injection of λ-carrageenan (30 μl of 1% (w/v) in sterile saline) into the right hind paw using an insulin syringe with a 28-gauge needle (di Meglio et al., 2005). Footpad thickness was measured with a digital caliper (FV Fowler Co., Newton, MA) immediately before injection. Three measurements of the same paw were taken subsequently every day for 11 days and compared with the initial readings. The increase in footpad thickness was considered to be edema. The rate of edema resolution was determined for each mouse using linear regression analysis of paw thickness from day 4 to day 11.

Determination of hyaluronic acid (HA) levels

Mice were euthanized 4 days post carrageenan injection, and their untreated and injected hind paws were severed. Half of each paw was freeze-dried for 16 hours, weighed and digested overnight at 60°C with papain (180 μg, Sigma) in 500 μl digestion buffer (0.2 M sodium acetate, 10 mM EDTA, pH 5.8). Papain was inactivated with 5 μl of iodoacetic acid (0.5 M) and samples were centrifuged at 4°C for 15 min. The supernatant was diluted 100 fold with digestion buffer and 10 μl was used to determine the HA levels by using the HA Test Kit (Corgenix Medical Corporation, Broomfield, CO) according to the manufacturer's instructions.

Histological Analysis of Mouse Tissues

Three pairs of male and female littermates with wild-type, *LYVE-1*$^{-/-}$, *CD44*$^{-/-}$ and *LYVE-1*$^{-/-}$/*CD44*$^{-/-}$ genotypes were sacrificed by CO_2 inhalation at two months of age. Tissues from multiple organs were collected and fixed in Bouin's solution, subjected to hematoxylin and eosin staining, and examined by microscopy. These organs include skin, muscle, liver, heart, lungs, brain, spleen, stomach, intestine, kidney and bone.

Immunohistochemistry to detect VEGFR-3 expression was performed as described with minor modifications (Kubo et al., 2000). Briefly, histological slides, 4 μm in thickness, were deparaffinized in xylene and a graded ethanol series, and antigen retrieval was achieved by heating in Cytomation Target Retrieval solution (DAKO, Glostrup, Denmark) for 10 minutes

in a microwave oven. After cooling for 20 minutes at room temperature, endogenous peroxidase was blocked with 3% hydrogen peroxide. Slides were incubated for 1 hour with 3% BSA/TBS-T at room temperature, prior to incubation overnight with rat anti-mouse-VEGFR-3 AFL4 -biotinylated antibodies (10 ug/ml, eBioscience, Inc, San Diego) in TBS-T/1% BSA at 4°C. Positive staining for VEGFR-3 was detected using the ABC kit (Vector Laboratories, Burlingame, CA) and counterstaining was performed using hematoxylin.

Immunohistochemistry to detect podoplanin expression was performed using a hamster anti-mouse podoplanin antibody (AngioBio, Del Mar, CA) and the Tyramide Signal Amplification Biotin System (PerkinElmer LAS, Inc., Waltham, MA) according to the manufacture's instructions with minor modifications. Following deparafinization, endogenous peroxidase activity was blocked with 1% hydrogen peroxide-methanol solution, and antigen retrieval was achieved by incubation with proteinase K. Sections were incubated with TNB blocking buffer for 30 minutes at room temperature, prior to overnight incubation at 4°C with anti-podoplanin antibody at 1:200 dilution in TNB buffer. After PBS washes, sections were then incubated with HRP-conjugated rabbit anti-syrian hamster IgG (Southern Biotech), biotinylated-tyramide and Streptavidin-HRP. Positive staining for podoplanin was detected with liquid DAB (DAKO Cytomation) and counterstaining was performed using hematoxylin.

Thioglycollate-induced peritonitis

Peritonitis was induced with an intraperitoneal injection of 1 ml of sterile thioglycollate (3%). Four days post injection, mice were euthanised by cervical dislocation and peritoneal lavage was performed with 8ml Hank's Balanced Salt Solution (Invitrogen, Carlsbad, CA) containing 10 mM Hepes and 5 mM EDTA as previously described (Moore et al., 2000). Briefly, collected cells were centrifuged, re-suspended in Red Blood Cell Lysis Buffer (Sigma-Aldrich) and counted using trypan blue exclusion on a hemocytometer. Collected cells were also cyto-spun onto glass slides and subjected to differential staining using the Diff Quick Stain Kit (IMEB Inc, San Marcos, CA) according to the manufacturer's instructions. For differential cell count, random areas of H&E/cytospun cells were imaged with a digital camera. The number of macrophages, PMNs and T cells in these images were then quantified.

Statistics

Quantitative data are presented as the mean ± SEM. Paired and unpaired Student's t test, Mann-Whitney U-test, ANOVA with Games-Howell post-hoc test and least squares linear regression were used for statistical analysis. Values of $p \leq 0.05$ were considered statistically significant.

RESULTS

Generation of LYVE-1-deficient mice

To investigate the *in vivo* function of LYVE-1, we generated a targeting construct designed to inactivate LYVE-1 by deleting exons 2 and 3, which encode the HA-binding Link domain (Fig. 1A). Correct targeting of the LYVE-1 locus in ES cells was verified by Southern blot analysis (Fig. 1B). Heterozygous mice were crossed, and the genotypes of the offspring were determined by PCR analysis (Fig. 1C). To determine whether replacement of exons 2 and 3 with a PGK-*neo*^{r} cassette altered the synthesis of LYVE-1 protein in mice carrying the mutant allele, Western blot analysis (Fig. 1D) was performed using antisera raised against peptides in the intracellular domain that have not been deleted by the targeting vector. LYVE-1 protein was detected in lung tissue from wild-type and heterozygous mice as a single band migrating with an apparent molecular mass of 60 kD, which is consistent with the migration of full-length protein (Banerji et al., 1999). In contrast, no LYVE-1 protein was detected in tissues obtained from homozygous mutant (LYVE-1$^{-/-}$) mice, indicating that these mice are LYVE-1-deficient. The genotypes of offspring from LYVE$^{+/-}$ pair matings indicate that the mutation is transmitted

to heterozygous and homozygous offspring at the expected frequency (21% wild-type, 53% *Lyve-1*$^{+/-}$ and 26% *Lyve-1*$^{-/-}$, N=80). The average litter size is 7.3 (80 pups from 11 litters), which is in the normal range for mice with 129/B6 mixed genetic background. LYVE-1$^{-/-}$ mice are viable, healthy, fertile and also produce litters of normal size (7.3 pups per litter) during their first year of life. They appear indistinguishable from their heterozygous and wild-type littermates. Histological analysis of multiple organs (see Materials and Methods) did not reveal any abnormalities in tissue architecture in both male and female LYVE-1$^{-/-}$ mice.

Generation of LYVE-1 and CD44 double knockout mice

Because LYVE-1 has high similarity (43%) to CD44, we tested the hypothesis that CD44 can compensate for the absence of LYVE-1 (Gale et al., 2007) by generating *LYVE-1/CD44* double knockout mice. Similar to *LYVE-1*-deficient mice, *CD44*-deficient mice also appear to be indistinguishable from wild-type mice under normal conditions (Protin et al., 1999; Schmits et al., 1997). Wild-type, *LYVE-1*$^{-/-}$,CD44$^{-/-}$ and *LYVE-1*$^{-/-}$/*CD44*$^{-/-}$ were obtained from mating of double heterozygous mice. The appearance and the average body weight (Table 1) of age and sex-matched adult wild-type, LYVE-1$^{-/-}$, CD44$^{-/-}$ and LYVE-1$^{-/-}$/CD44$^{-/-}$ were similar. Macroscopic manifestations of defective lymphatic function such as skin edema and chylous accumulation in the abdominal, pleural or pericardial cavities were not observed in any of these mice. No edema in the hind paws was evident (Table 1), although slight variations in the paws of wild-type, *LYVE-1*$^{-/-}$, *CD44*$^{-/-}$ and *LYVE-1*$^{-/-}$/*CD44*$^{-/-}$ mice were resolved.

Structure of lymphatic vessels and their uptake of macromolecules are normal in *LYVE-1* and/or *CD44*-deficient mice

To determine whether the structure of lymphatic vessels is affected by the absence of LYVE-1 and/or CD44, we performed microlymphangiography by injecting FITC-dextran intradermally into the mouse tail. The regular, hexagonal network of superficial lymphatic vessels in this region allows for assessment of abnormalities in vessel location, density and diameter. The typical hexagonal pattern was detected in both wild-type and LYVE-1$^{-/-}$ mice (Fig. 2A) as well as CD44$^{-/-}$ and LYVE-1$^{-/-}$/CD44$^{-/-}$ mice (not shown). Lymphatic vessel diameter and density were not significantly different between wild-type, LYVE-1$^{-/-}$, CD44$^{-/-}$ and LYVE-1$^{-/-}$/CD44$^{-/-}$ mice (Table 2). In addition, the morphology and density of ear lymphatic vessels appear comparable in wild-type, LYVE-1$^{-/-}$, CD44$^{-/-}$ and LYVE-1$^{-/-}$/CD44$^{-/-}$ mice (Fig. 2B).

To investigate whether lymphatic vessels in *LYVE-1* and/or *CD44*-deficient mice are altered at the morphological level, we performed histological analysis of several tissues using antisera raised against VEGFR-3 and podoplanin. Our staining of mouse kidneys (Fig. 3A), lungs and liver (data not shown) detected VEGFR-3-positive lymphatic vessels that are similar in appearance, structure and location in wild-type, *LYVE-1*$^{-/-}$, *CD44*$^{-/-}$ and *LYVE-1*$^{-/-}$/*CD44*$^{-/-}$ mice. Lymphatic vessels detected with an anti-podoplanin antibody also appear similar in liver tissues (Fig. 3B), kidneys and skin (data not shown) of wild-type, *LYVE-1*$^{-/-}$, *CD44*$^{-/-}$ and *LYVE-1*$^{-/-}$ /*CD44*$^{-/-}$ mice. Together, these results indicate that both LYVE-1 and CD44 are dispensable for normal lymphatic development and the uptake and transport of macromolecular dextrans in lymphatic vessels, as well as for the structure and morphology of normal lymphatic vessels.

Transport by lymphatic vessels is unaffected by *LYVE-1* and/or *CD44* deletion

To maintain tissue homeostasis, lymphatic vessels are not only required to take up extracellular fluid and macromolecules, but also to return these components to the venous circulation. Because the initial lymphatic endothelium in adults retains LYVE-1 expression, we postulated that LYVE-1 might have a role in regulating lymph production and transport. We performed fluorescence microlymphangiography in the mouse tail, and used the residence time

distribution theory to calculate lymph fluid velocity (Swartz et al., 1996) to determine whether lymph flow is altered by the absence of LYVE-1 and/or CD44. The overall lymphatic fluid velocities in wildtype (10.5 ± 1.0 μm/s, n=8,), *LYVE-1*$^{-/-}$ (8.9 ± 1.1 μm/s, n=7), *CD44*$^{-/-}$ (10.8 ± 1.0 μm/s, n=8) and *LYVE-1*$^{-/-}$ /*CD44*$^{-/-}$ (8.5 ± 1.0 μm/s, n=8) mice are not significantly different from each other ($p > 0.3$; Fig. 4A). These values are comparable to previously published lymphatic velocities in C57BL/6 mice (Hagendoorn et al., 2004). Taken together, these findings indicate that transport of lymph and macromolecular dextrans in lymphatic vessels is not significantly affected by LYVE-1 and/or CD44 deficiency.

LYVE-1$^{-/-}$/*CD44*$^{-/-}$ mice may show subtle inflammatory phenotype

Although LYVE-1 and CD44 do not appear to regulate lymphatic vessel morphology or lymph transport under normal conditions, they may regulate these functions during pathological processes such as tissue injury and inflammation. Under inflammatory conditions, release of histamine, kinins and other molecules by damaged cells and recruited leukocytes cause vasodilation and increased permeability of local blood vessels, which can lead to tissue edema. Resolution of edema is achieved by uptake of excess interstitial fluid by vascular and lymphatic vessels and a reduction in vascular permeability. CD44 expression on leukocytes and endothelial cells has been shown to facilitate leukocyte transmigration at sites of inflammation where HA synthesis is upregulated (Protin et al., 1999; Teder et al., 2002). Because LYVE-1 has been shown to bind and internalize HA *in vitro*, it is possible that LYVE-1 expressed on the lymphatic endothelium is involved in regulating the extent and duration of edema by limiting leukocyte/HA interaction. To determine the role of LYVE-1 and CD44 under inflammatory conditions, we injected polysaccharide λ-carrageenan into the footpad of the mouse hind leg, which has been shown to induce inflammation that is accompanied by leukocyte infiltration and tissue edema (di Meglio et al., 2005; Fernandes and Assreuy, 2004). Our daily measurements did not resolve the early peak (0 to 6 hours) in edema that occurs with λ-carrageenan injections and show that edema in all mice is maximal 3–4 days post injection. The longer time to maximal edema in our animal model compared to other published studies (*e.g.* di Meglio et al., 2005; Fernandes and Assreuy, 2004) is likely related to the mixed background 129/C57BL6 mice used in this study and is in line with other published data (Posadas et al., 2004). Wild-type and LYVE-1-deficient mice responded similarly to λ-carrageenan injection (Fig. 4B). Comparable paw edema was also observed in *CD44*-deficient mice (Fig. 4B), which is consistent with a previous study that showed comparable edema in wild-type and *CD44*$^{-/-}$ mice resulting from footpad injection of LCMV (Schmits et al., 1997). Interestingly, mice deficient for both CD44 and LYVE-1 showed a subtle, but significant, increase in paw swelling compared to wild-type mice near the peak of edema ($p < 0.05$, day 5) (Fig. 4B). However, on day 4 this difference could not be resolved either using the paw thickness measurements or using weight/dry ratios (data not shown). However, animals were not age matched and there was significant variability within each of the four groups tested. Age dependency on the maximum paw thickness in λ-carrageenan injected mice has been documented (Posadas et al., 2004), and is consistent with our data (not shown). Mice deficient for both CD44 and LYVE-1 were on average 30% older than their wildtype counterparts at the time of λ-carrageenan injection, potentially explaining the subtle phenotype observed.

Edema is resolved at comparable rates in all mice (0.11 ± 0.01 mm/day for wild-type mice; 0.10 ± 0.01 mm/day for *LYVE-1*$^{-/-}$ mice; 0.10± 0.02 mm/day for *CD44*$^{-/-}$ mice; and 0.13 ± 0.02 mm/day for *LYVE-1*$^{-/-}$/*CD44*$^{-/-}$ mice), suggesting that LYVE-1 and CD44 are not required for resolution of inflammation in this model. To determine whether elevated levels of proinflammatory HA contribute to increased swelling in double knockout mice, we measured HA levels in paws on day 4 during maximal edema using an HA test kit (Fig. 4C). Our results show no difference in HA levels comparing wild-type, *LYVE-1*$^{-/-}$, *CD44*$^{-/-}$ and *LYVE-1*$^{-/-}$/$^{CD44-/-}$ mice ($p > 0.5$).

LYVE-1 may be important to leukocyte recruitment as has been shown previously for CD44 (Protin et al., 1999). To quantitatively assess leukocyte recruitment during inflammation, we used the thioglycollate-induced peritonitis model, which has been shown to induce the recruitment of macrophages, polymorphic neutrophils (PMNs) and lymphocytes to the peritoneum (Potter et al., 2003). We performed peritoneal lavage four days after intraperitoneal injection of thioglycollate to collect maximal numbers of recruited leukocytes (Potter et al., 2003). We extracted $8.8 \pm 1.2 \times 10^6$ cells from wild-type mice (Fig. 4D), which is consistent with published studies (Potter et al., 2003). A comparable number of cells ($8.1 \pm 0.6 \times 10^6$) were collected from *LYVE-1*$^{-/-}$ mice (Fig. 4D). About 40% more cells were collected from *CD44*$^{-/-}$ mice ($11.2 \pm 2.4 \times 10^6$) and from *LYVE-1*$^{-/-}$/*CD44*$^{-/-}$ mice ($12.1 \pm 2.5 \times 10^6$), but these results were not statistically significant ($p > 0.05$). Our experiments were powered to detect a difference of 75%, thus this subtle difference could not be statistically resolved with our experimental design. To investigate whether recruited leukocytes in double knockout mice have altered subpopulations, we performed differential staining of collected cells with Giemsa to quantify macrophages, PMNs and lymphocytes. Consistent with previous studies (Potter et al., 2003), macrophages are the most abundant cell type at this phase of inflammation. We found no significant difference in the leukocyte subpopulations collected from the different mice (Fig. 4E). Taken together, these results suggest that LYVE-1 does not regulate inflammation via leukocyte recruitment to the affected area.

DISCUSSION

We originally expected that LYVE-1 is involved in the development of the lymphatic system or the regulation of its function because LYVE-1 is expressed in embryonic lymphatic endothelium, as well as in adult initial lymphatic vessels. Abnormalities in the development or function of the lymphatics may manifest as tissue edema and chylous accumulation in the intestines or peritoneal cavity, as was observed in mice lacking the homeobox protein Prox1 (Wigle and Oliver, 1999) and the plasma membrane protein podoplanin (Schacht et al., 2003). Since both these proteins have expression patterns in the lymphatics similar to that of LYVE-1 (Wigle and Oliver, 1999), we were surprised by the absence of lymphedema and chylous ascites in LYVE-1-deficient mice. Gale and colleagues have also shown the lack of lymphatic phenotype in LYVE-1 null mice (Gale et al., 2007). These findings prompted us to determine whether LYVE-1 function in the knockout mice is compensated by CD44, the closest homologue of LYVE-1. Lymphatic vessels in *LYVE-1* and/or *CD44*-deficient mice have normal lymphatic vessel diameter, network morphology, and location and expression of the lymphatic marker podoplanin. We also found no perturbations in lymph flow velocity under normal conditions. These functional and morphological studies suggest either that LYVE-1 and CD44 are not necessary for development of a functional lymphatic system, or that LYVE-1/CD44 functions are compensated by other molecules. Although CD44 is the closest homologue of LYVE-1, its expression is normally absent in lymphatic vasculature and not induced in lymphatics of LYVE-1 knockout mice (Gale et al., 2007). It is possible that compensation of LYVE-1 function in lymphatics is achieved by a similarly functioning molecule yet to be identified. A recent report showed that LYVE-1 is expressed on lymphatic capillaries that are not associated with smooth muscle cells, and the dissociation of smooth muscle cells increased LYVE-1 expression in collecting lymphatics (Tammela et al., 2007). These data suggest that LYVE-1 is not necessary to maintain lymphatic identity of the endothelium. Although LYVE-1 likely has a specific function in lymphatic endothelium that has yet to be determined, it is clear that LYVE-1 is not a regulator of lymphatic identity in general.

Because LYVE-1 has high sequence similarity to CD44, an HA-receptor that has been shown to be essential for leukocyte recruitment to sites of inflammation and for the resolution of lung inflammation (Gee et al., 2004; Teder et al., 2002; Weber et al., 2002), we investigated whether LYVE-1 is involved in regulating inflammation. Using the λ-carrageenan-induced paw edema

model, we observed no significant differences in the extent or duration of edema in *LYVE-1*$^{-/-}$, *CD44*$^{-/-}$ and wild-type mice (Fig. 4B). Although *LYVE-1*$^{-/-}$/*CD44*$^{-/-}$ mice exhibit a similar time course for the resolution of inflammation, they manifested significantly enhanced edema near the peak of inflammation (Fig. 4B). Increased edema in double knockout mice does not seem to be due to defective lymphatic function, since resolution of edema occurred at comparable rates in all four genotypes of mice in our study, but may be attributed to the older age of double knockout mice at the time of λ-carrageenan injection.

Several other factors may contribute to the observed increased edema, including enhanced levels of pro-inflammatory HA, which has been shown to facilitate leukocyte recruitment to sites of inflammation (DeGrendele et al., 1997; Mohamadzadeh et al., 1998; Nandi et al., 2000). However, we did not see an increase in HA in the λ-carrageenan-induced paw edema model (Fig. 4C). Using the thioglycollate-induced peritonitis model to quantitatively assess leukocyte recruitment, we observed no difference in the number of cells collected from wild-type and LYVE-1$^{-/-}$ mice (Fig. 4D). However, we did detect a trend toward an increase in recruited cells in CD44$^{-/-}$ mice (Fig. 4D), which is consistent with previous findings of increased recruitment of macrophages, PMNs and lymphocytes in a bleomycin-induced lung inflammation model (Teder et al., 2002). In the absence of both *LYVE-1* and *CD44*, a similar increase in recruitment of leukocytes to the peritoneum was observed. Taken together we speculate that CD44 deficiency is a component of somewhat increased inflammatory response in the double knockout mice.

The functional role for LYVE-1 in the lymphatic system still remains a mystery. As its function in inflammation becomes known, its role in the lymphatic system will become clearer.

ACKNOWLEDGEMENTS

This study was supported by the National Institute of Health (R01-CA85140, P01-CA80124 and U01-CA84301). The authors thank Drs. Emmanuelle di Tomaso for constructive comments; and Michele Riley and Mingtau Lee for technical assistance.

Grant Information:

Contract grant sponsor: National Institute of Health: Contract grant number: R01-CA85140

Contract grant sponsor: National Institute of Health: Contract grant number: P01-CA80124

Contract grant sponsor: National Institute of Health: Contract grant number: U01-CA84301

REFERENCES

Achen MG, McColl BK, Stacker SA. Focus on lymphangiogenesis in tumor metastasis. Cancer Cell 2005;7(2):121–127. [PubMed: 15710325]

Alitalo K, Carmeliet P. Molecular mechanisms of lymphangiogenesis in health and disease. Cancer Cell 2002;1(3):219–227. [PubMed: 12086857]

Banerji S, Ni J, Wang SX, Clasper S, Su J, Tammi R, Jones M, Jackson DG. LYVE-1, a new homologue of the CD44 glycoprotein, is a lymph-specific receptor for hyaluronan. J Cell Biol 1999;144(4):789–801. [PubMed: 10037799]

DeGrendele HC, Estess P, Siegelman MH. Requirement for CD44 in activated T cell extravasation into an inflammatory site. Science 1997;278(5338):672–675. [PubMed: 9381175]

di Meglio P, Ianaro A, Ghosh S. Amelioration of acute inflammation by systemic administration of a cell-permeable peptide inhibitor of NF-kappaB activation. Arthritis Rheum 2005;52(3):951–958. [PubMed: 15751079]

Fernandes D, Assreuy J. Involvement of guanylate cyclase and potassium channels on the delayed phase of mouse carrageenan-induced paw oedema. Eur J Pharmacol 2004;501(1–3):209–214. [PubMed: 15464080]

Gale NW, Prevo R, Espinosa J, Ferguson DJ, Dominguez MG, Yancopoulos GD, Thurston G, Jackson DG. Normal lymphatic development and function in mice deficient for the lymphatic hyaluronan receptor LYVE-1. Mol Cell Biol 2007;27(2):595–604. [PubMed: 17101772]

Gee K, Kryworuchko M, Kumar A. Recent advances in the regulation of CD44 expression and its role in inflammation and autoimmune diseases. Arch Immunol Ther Exp (Warsz) 2004;52(1):13–26. [PubMed: 15053229]

Gordon EJ, Gale NW, Harvey NL. Expression of the hyaluronan receptor LYVE-1 is not restricted to the lymphatic vasculature; LYVE-1 is also expressed on embryonic blood vessels. Dev Dyn 2008;237 (7):1901–1909. [PubMed: 18570254]

Hagendoorn J, Padera TP, Kashiwagi S, Isaka N, Noda F, Lin MI, Huang PL, Sessa WC, Fukumura D, Jain RK. Endothelial nitric oxide synthase regulates microlymphatic flow via collecting lymphatics. Circ Res 2004;95(2):204–209. [PubMed: 15192027]

Jackson DG. Biology of the lymphatic marker LYVE-1 and applications in research into lymphatic trafficking and lymphangiogenesis. Apmis 2004;112(7–8):526–538. [PubMed: 15563314]

Jeltsch M, Kaipainen A, Joukov V, Meng X, Lakso M, Rauvala H, Swartz M, Fukumura D, Jain RK, Alitalo K. Hyperplasia of lymphatic vessels in VEGF-C transgenic mice. Science 1997;276(5317): 1423–1425. [PubMed: 9162011]

Karkkainen MJ, Haiko P, Sainio K, Partanen J, Taipale J, Petrova TV, Jeltsch M, Jackson DG, Talikka M, Rauvala H, Betsholtz C, Alitalo K. Vascular endothelial growth factor C is required for sprouting of the first lymphatic vessels from embryonic veins. Nat Immunol 2004;5(1):74–80. [PubMed: 14634646]

Knudson CB, Knudson W. Hyaluronan-binding proteins in development, tissue homeostasis, and disease. Faseb J 1993;7(13):1233–1241. [PubMed: 7691670]

Kubo H, Fujiwara T, Jussila L, Hashi H, Ogawa M, Shimizu K, Awane M, Sakai Y, Takabayashi A, Alitalo K, Yamaoka Y, Nishikawa SI. Involvement of vascular endothelial growth factor receptor-3 in maintenance of integrity of endothelial cell lining during tumor angiogenesis. Blood 2000;96(2): 546–553. [PubMed: 10887117]

Lee EC, Yu D, Martinez de Velasco J, Tessarollo L, Swing DA, Court DL, Jenkins NA, Copeland NG. A highly efficient Escherichia coli-based chromosome engineering system adapted for recombinogenic targeting and subcloning of BAC DNA. Genomics 2001;73(1):56–65. [PubMed: 11352566]

Makinen T, Adams RH, Bailey J, Lu Q, Ziemiecki A, Alitalo K, Klein R, Wilkinson GA. PDZ interaction site in ephrinB2 is required for the remodeling of lymphatic vasculature. Genes Dev 2005;19(3):397–410. [PubMed: 15687262]

McKee CM, Penno MB, Cowman M, Burdick MD, Strieter RM, Bao C, Noble PW. Hyaluronan (HA) fragments induce chemokine gene expression in alveolar macrophages. The role of HA size and CD44. J Clin Invest 1996;98(10):2403–2413. [PubMed: 8941660]

Mohamadzadeh M, DeGrendele H, Arizpe H, Estess P, Siegelman M. Proinflammatory stimuli regulate endothelial hyaluronan expression and CD44/HA-dependent primary adhesion. J Clin Invest 1998;101(1):97–108. [PubMed: 9421471]

Moore KJ, Andersson LP, Ingalls RR, Monks BG, Li R, Arnaout MA, Golenbock DT, Freeman MW. Divergent response to LPS and bacteria in CD14-deficient murine macrophages. J Immunol 2000;165 (8):4272–4280. [PubMed: 11035061]

Mouta Carreira C, Nasser SM, di Tomaso E, Padera TP, Boucher Y, Tomarev SI, Jain RK. LYVE-1 is not restricted to the lymph vessels: expression in normal liver blood sinusoids and down-regulation in human liver cancer and cirrhosis. Cancer Res 2001;61(22):8079–8084. [PubMed: 11719431]

Nandi A, Estess P, Siegelman MH. Hyaluronan anchoring and regulation on the surface of vascular endothelial cells is mediated through the functionally active form of CD44. J Biol Chem 2000;275 (20):14939–14948. [PubMed: 10809739]

Nelson GM, Padera TP, Garkavtsev I, Shioda T, Jain RK. Differential gene expression of primary cultured lymphatic and blood vascular endothelial cells. Neoplasia 2007;9(12):1038–1045. [PubMed: 18084611]

Posadas I, Bucci M, Roviezzo F, Rossi A, Parente L, Sautebin L, Cirino G. Carrageenan-induced mouse paw oedema is biphasic, age-weight dependent and displays differential nitric oxide cyclooxygenase-2 expression. Br J Pharmacol 2004;142(2):331–338. [PubMed: 15155540]

Potter PK, Cortes-Hernandez J, Quartier P, Bottox M, Walport MJ. Lupus-prone mice have an abnormal response to thioglycolate and an impaired clearance of apoptotic cells. Journal of Immunology 2003;170:3223–3232.

Prevo R, Banerji S, Ferguson DJ, Clasper S, Jackson DG. Mouse LYVE-1 is an endocytic receptor for hyaluronan in lymphatic endothelium. J Biol Chem 2001;276(22):19420–19430. [PubMed: 11278811]

Protin U, Schweighoffer T, Jochum W, Hilberg F. CD44-deficient mice develop normally with changes in subpopulations and recirculation of lymphocyte subsets. J Immunol 1999;163(9):4917–4923. [PubMed: 10528194]

Saharinen P, Tammela T, Karkkainen MJ, Alitalo K. Lymphatic vasculature: development, molecular regulation and role in tumor metastasis and inflammation. Trends Immunol 2004;25(7):387–395. [PubMed: 15207507]

Schacht V, Ramirez MI, Hong YK, Hirakawa S, Feng D, Harvey N, Williams M, Dvorak AM, Dvorak HF, Oliver G, Detmar M. T1alpha/podoplanin deficiency disrupts normal lymphatic vasculature formation and causes lymphedema. Embo J 2003;22(14):3546–3556. [PubMed: 12853470]

Schmid-Schonbein GW. Microlymphatics and lymph flow. Physiol Rev 1990;70(4):987–1028. [PubMed: 2217560]

Schmits R, Filmus J, Gerwin N, Senaldi G, Kiefer F, Kundig T, Wakeham A, Shahinian A, Catzavelos C, Rak J, Furlonger C, Zakarian A, Simard JJ, Ohashi PS, Paige CJ, Gutierrez-Ramos JC, Mak TW. CD44 regulates hematopoietic progenitor distribution, granuloma formation, and tumorigenicity. Blood 1997;90(6):2217–2233. [PubMed: 9310473]

Swartz MA, Berk DA, Jain RK. Transport in lymphatic capillaries. I. Macroscopic measurements using residence time distribution theory. Am J Physiol 1996;270(1 Pt 2):H324–H329. [PubMed: 8769768]

Tammela T, Saaristo A, Holopainen T, Lyytikka J, Kotronen A, Pitkonen M, Abo-Ramadan U, Yla-Herttuala S, Petrova TV, Alitalo K. Therapeutic differentiation and maturation of lymphatic vessels after lymph node dissection and transplantation. Nat Med 2007;13(12):1458–1466. [PubMed: 18059280]

Teder P, Vandivier RW, Jiang D, Liang J, Cohn L, Pure E, Henson PM, Noble PW. Resolution of lung inflammation by CD44. Science 2002;296(5565):155–158. [PubMed: 11935029]

Termeer CC, Hennies J, Voith U, Ahrens T, Weiss JM, Prehm P, Simon JC. Oligosaccharides of hyaluronan are potent activators of dendritic cells. J Immunol 2000;165(4):1863–1870. [PubMed: 10925265]

Weber GF, Bronson RT, Ilagan J, Cantor H, Schmits R, Mak TW. Absence of the CD44 gene prevents sarcoma metastasis. Cancer Res 2002;62(8):2281–2286. [PubMed: 11956084]

West DC, Hampson IN, Arnold F, Kumar S. Angiogenesis induced by degradation products of hyaluronic acid. Science 1985;228(4705):1324–1326. [PubMed: 2408340]

Wigle JT, Harvey N, Detmar M, Lagutina I, Grosveld G, Gunn MD, Jackson DG, Oliver G. An essential role for Prox1 in the induction of the lymphatic endothelial cell phenotype. Embo J 2002;21(7):1505–1513. [PubMed: 11927535]

Wigle JT, Oliver G. Prox1 function is required for the development of the murine lymphatic system. Cell 1999;98(6):769–778. [PubMed: 10499794]

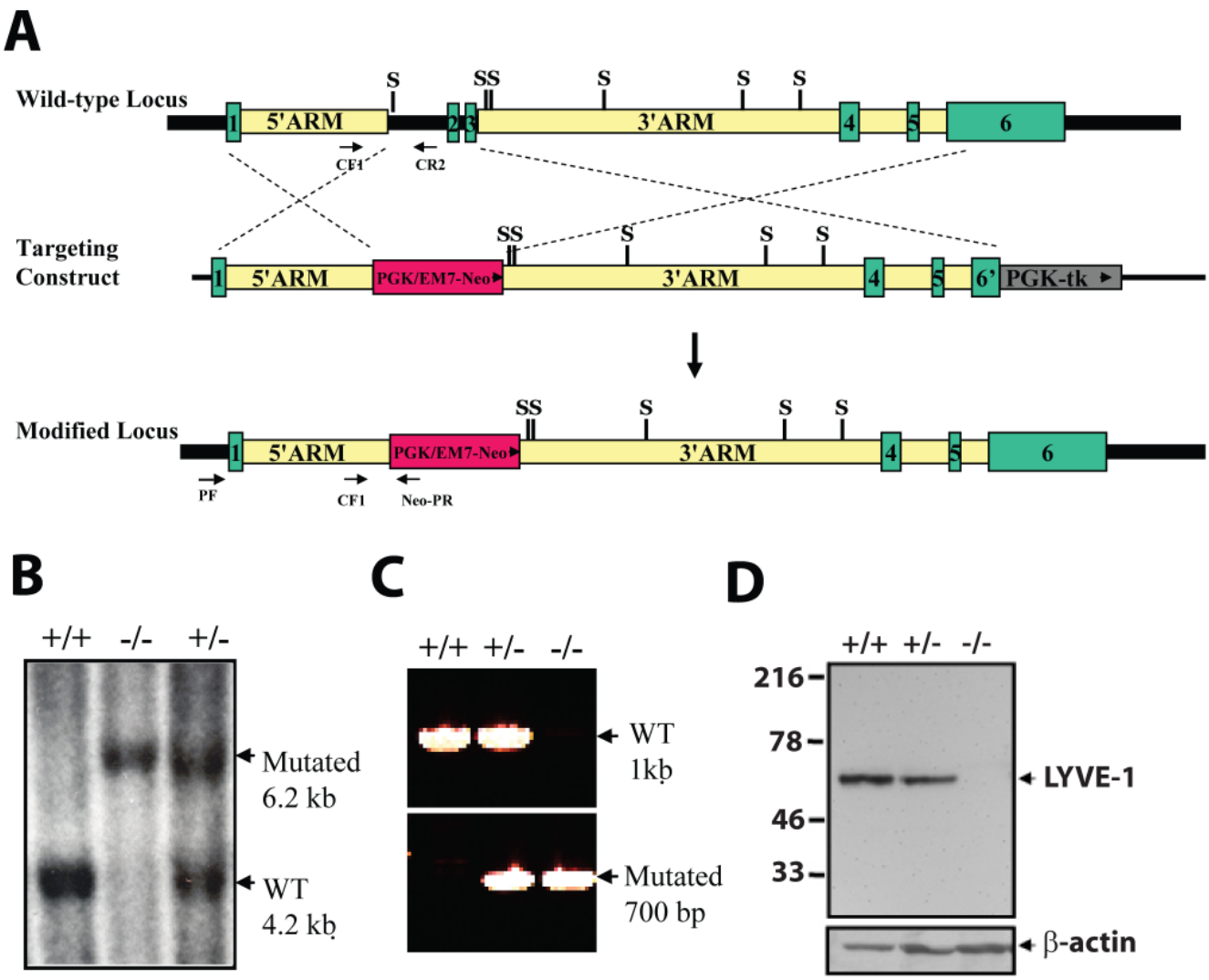

FIG. 1. Targeted inactivation of the mouse *LYVE-1* gene

(A) Schematic diagram of the *LYVE-1* locus, the targeting construct and the mutant allele. Homologous recombination of the targeting vector introduces the *neo* gene downstream of the *LYVE-1* promoter, deleting exons 2 and 3 of the *LYVE-1* gene. Green boxes indicate the coding exons, whereas the dashed lines indicate the regions of identity between the *LYVE-1* locus and the targeting vector. *tk*, selectable thymidine kinase gene; WT, wild-type. S, *Ssp*I. (B) Southern blot analysis of *Ssp*I-digested genomic DNA from targeted ES cells using an 856-bp 5' external probe generated from PCR primers UF and UR. A 6.2-kb restriction fragment is diagnostic for the mutated allele, whereas a 4.2-kb fragment is generated from the wild-type allele. +/+, wild-type; +/−, heterozygous; −/−, homozygous mutant. (C) Genotyping by PCR analysis of genomic tail DNA. Primer pairs CF1/CR2 and CF1/neo-PR were used to detect the wild-type and mutant alleles, respectively. (D) Western blot analysis of proteins (20 μg) from lung tissue using LYVE-1 antibody detects a 60-kD band in wild-type and heterozygous samples, but not in homozygous mutant samples.

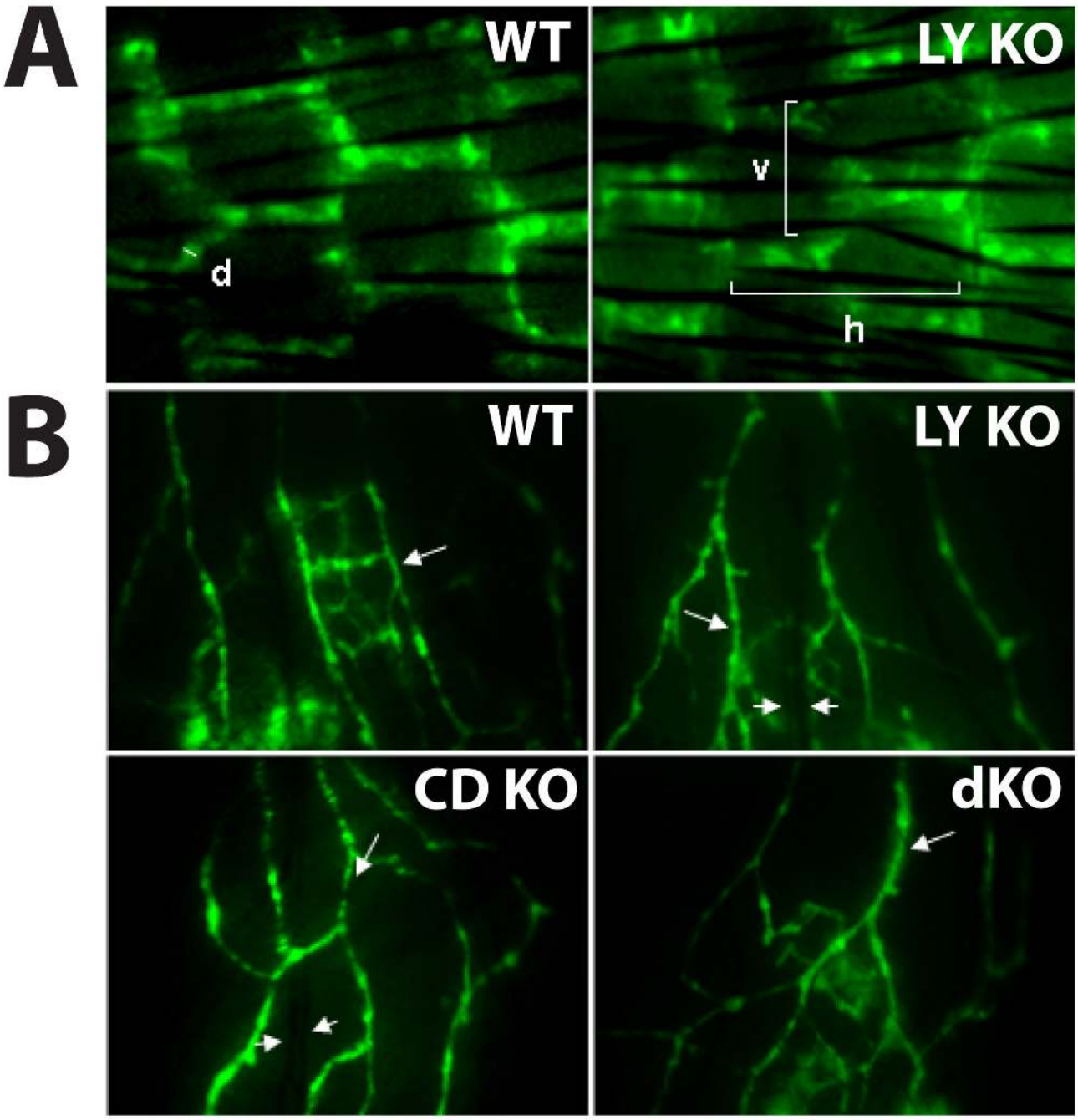

FIG. 2. Visualization of lymphatic vessels by fluorescent lymphangiography

FITC-dextran of 2 million Da was injected subcutaneously into the tail (A) and ear (B) of wild-type and mutant mice. Vessels were imaged using fluorescent microscopy. (A) The measured parameters are vessel diameter (d), and horizontal (h) and vertical (v) mesh sizes. (B) Arrows indicate fluorescent lymphatic vessels in the mouse ear, whereas arrowheads indicate blood vessels. Results shown are from 1 mouse in each group representative of 5 mice per group. WT = wild-type; LY KO = *LYVE-1*$^{-/-}$; CD KO = *CD44*$^{-/-}$; and dKO = *LYVE-1*$^{-/-}$/*CD44*$^{-/-}$. Images are 1.75 mm wide.

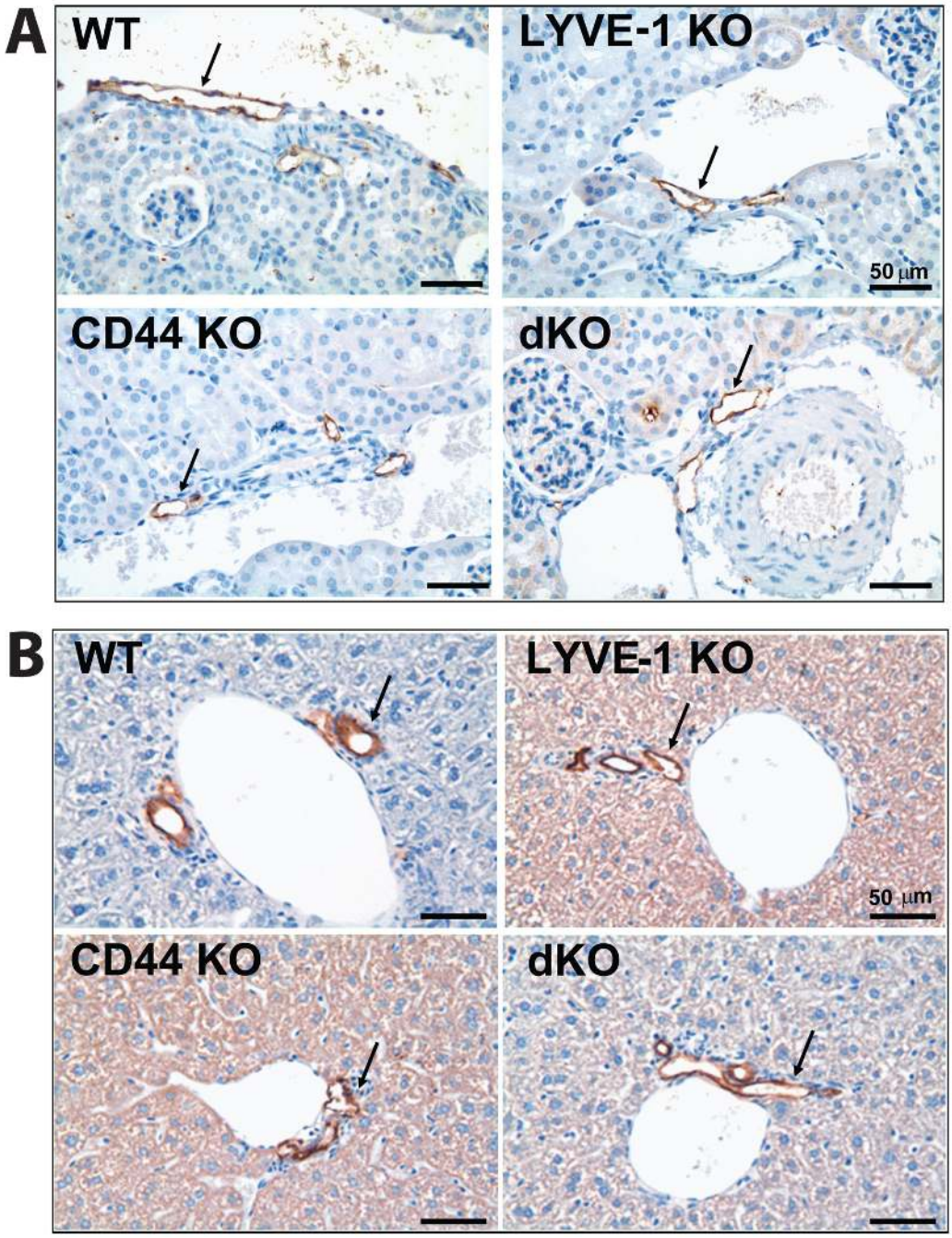

FIG. 3. Lymphatic vessels in wild-type and mutant mice

(A) Immunostaining of lymphatic vessels (arrows) with anti-VEGFR-3 monoclonal antibodies in kidney tissue show no differences in the four animal types. (B) Lymphatic vessels (arrows) in liver tissue appear similar in wild-type and mutant mice using immunostaining with anti-podoplanin antibodies. WT = wild-type; LY KO = *LYVE-1*$^{-/-}$; CD KO = *CD44*$^{-/-}$; and dKO = *LYVE-1*$^{-/-}$/*CD44*$^{-/-}$. Scale bar = 50 μm.

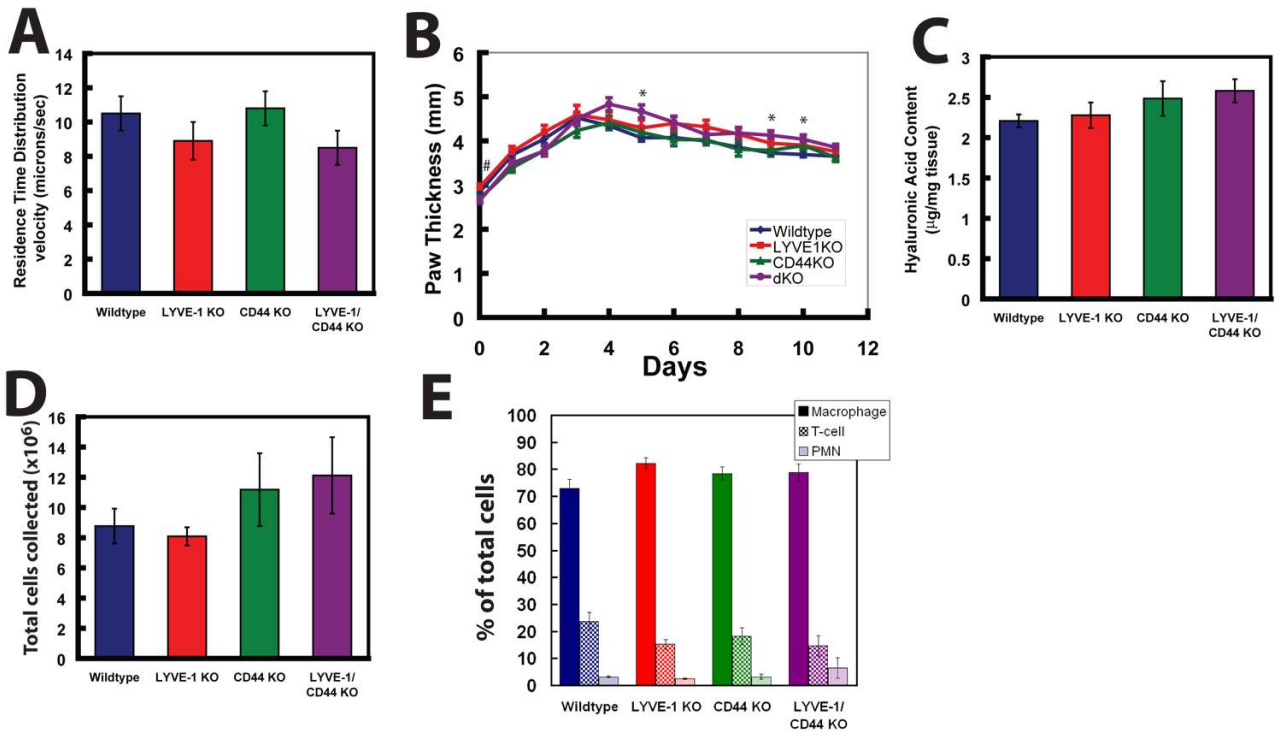

FIG. 4. Functional consequences of *LYVE-1* and *CD44* deficiency

A) Lymph flow velocity in the tail lymphatic vessel network in wild-type (n = 8), LYVE-1 KO (n =7) mice, CD44 KO (n = 8) and LYVE-1/CD44 double KO (n = 8) mice was determined by residence time distribution analysis and showed no difference amongst the four groups ($p > 0.3$). Data are presented as mean ± standard error. B) Carrageenan-induced paw edema is significantly enhanced in LYVE-1/CD44 double knockout mice. λ-carrageenan (30 µl) was injected into the right paw of mice and edema was determined by paw thickness during daily monitoring. WT (n = 20), LY KO (n =11) mice, CD44 KO (n = 7) and dKO (n = 9) mice. *$p < 0.05$ dKO compared to WT; #$p < 0.05$ dKO compared to LYVE-1 KO. (C) Paws were removed 4 days after λ-carrageenan injection, freeze-dried and hyaluronic acid levels were determined using an HA test kit. HA levels are expressed as µg HA protein per mg of dry weight tissue and showed no differences amongst the groups ($p < 0.05$). WT (n = 6), LY KO (n = 8), CD44 KO (n = 6) and dKO (n = 6). Data are presented as the mean ± standard error. D) Mice were given an intraperitoneal injection of thioglycollate and subjected to peritoneal lavage 4 days later. Total numbers of viable cells were counted by using trypan blue dye exclusion method. WT (n = 6), CD44 KO (n = 4), LY KO (n =7) and dKO (n = 3) mice. E) Cells were subjected to differential staining (Giemsa) and macrophages, polymorphic neutrophils (PMNs) and lymphocytes were counted. Data are presented as the mean ± standard error.

TABLE 1

Body weight and paw thickness in adult mice

Genotype	Body weight (g)	Paw Thickness (mm)
Wild-type	26 ± 1.3 (n=8)	2.8 ± 0.04 (n=26)
LYVE-1 $^{-/-}$	28 ± 1.8 (n=8)	2.9 ± 0.06 (n=19)
CD44 $^{-/-}$	25 ± 0.9 (n=8)	2.6 ± 0.05 (n=14) *
LYVE-1$^{-/-}$/*CD44*$^{-/-}$	26 ±1.2 (n=8)	2.6 ± 0.05 (n=18) *

Differences between wild-type and LYVE-1 and/or CD44-deficient mice for these parameters were determined by ANOVA analysis with Games-Howell post-hoc test.

* $p < 0.05$ when compared to paw thickness in LYVE-1$^{-/-}$ animals.

TABLE 2

Tail lymphatic vessel diameter and network morphology

Genotype	Lymphatic vessel diameter (μm)	Horizontal mesh size (μm)	Vertical mesh size (μm)
Wild-type (n=17)	48 ± 1	700 ± 8	280 ± 5
LYVE-1 $^{-/-}$ (n=9)	51 ± 3	660 ± 20	270 ± 4
CD44 $^{-/-}$ (n=7)	47 ± 1	660 ± 20	270 ± 8
LYVE-1$^{-/-}$//*CD44*$^{-/-}$ (n=14)	49 ± 2	680 ± 10	280 ± 4

There were no significant differences between wild-type, *LYVE-1* $^{-/-}$, *CD44* $^{-/-}$ and double knockout mice for these tail morphometric parameters, as determined by the ANOVA analysis with Games-Howell post-hoc test. The *p* values were greater than 0.4 in all cases.